Revision 2

Micro- and nano-scale textural and compositional zonation in plagioclase at the Black Mountain porphyry Cu deposit: implications for magmatic processes

MINGJIAN CAO[1,2,3*], NOREEN J. EVANS[3], STEVEN M. REDDY[3,4], DENIS FOUGEROUSE[3,4], PETE HOLLINGS[5], DAVID W. SAXEY[4], BRENT I.A. MCINNES[3], DAVID R. COOKE[6], BRAD J. MCDONALD[3], KEZHANG QIN[1,2]

[1]Key Laboratory of Mineral Resources, Institute of Geology and Geophysics, Chinese Academy of Sciences, P.O. Box 9825, Beijing 100029, China

[2]Institutions of Earth Science, Chinese Academy of Sciences, Beijing 100029, China

[3]John de Laeter Center/TIGeR/School of Earth and Planetary Science, Curtin University, Perth WA 6945, Australia

[4]Geoscience Atom Probe, Advanced Resource Characterisation Facility, John de Laeter Centre, Curtin University, GPO Box U1987, Perth, WA 6845, Australia

[5]Geology Department, Lakehead University, 955 Oliver Rd, Thunder Bay, ON, P7B 5E1, Canada

[6]ARC Research Hub for Transforming the Mining Value Chain & CODES, Centre for Ore Deposit and Exploration Science, University of Tasmania, Private Bag 126, Hobart, Tasmania 7001, Australia

Corresponding author: email: caomingjian@mail.iggcas.ac.cn

Abstract

Textural and compositional micro-scale (10-100μm) and nano-scale (10-100 nm) zoning in a plagioclase phenocryst from a fresh, syn-mineralization diorite porphyry (Black Mountain porphyry Cu-Au deposit, Phillipines) was characterized for major and trace elements using electron microprobe, laser ablation inductively coupled plasma mass spectrometry and atom probe tomography. The complex plagioclase crystal (3.0 × 5.4 mm) has a patchy andesine core (An_{41-48} mol%), eroded bytownite mantle (An_{71-80} mol%) and oscillatory andesine rim (An_{39-51} mol%). Micro-scale variations with a periodic width of 50 to 200 μm were noted for most major and trace elements (Si, Ca, Al, Na, K, Fe, Mg, Ti, Sr, Ba, Pb, La, Ce and Pr) with a ΔAn amplitude of 4-12 mol% in both the core and rim. The mantle has a distinct elemental composition, indicating the addition of hotter mafic magma to the andesitic magma. Atom probe tomography shows an absence of nano-scale variations in the andesine rim but alternating nano-scale (25-30 nm) Al-, Ca-rich and Si-, Na-rich zones with a $Ca/(Ca+Na)_{atom\,\%}$ amplitude of ~10 in the bytownite mantle.

The restricted variations in physiochemical parameters (H_2O-rich, T = 865 to 895 ºC, P = 5.3 to 6.2 kbar; fO_2 = NNO+0.6 to NNO+1.1 recorded by co-precipitated amphibole) suggest micro-scale oscillatory zoning was likely controlled by internal crystal growth mechanisms, and not by periodic variations in physiochemical conditions. However, the uniform diffusion timescale for CaAl-NaSi interdiffusion in the mantle is far shorter than the crystallization timescale of the grain from mantle to rim, suggesting nano-scale zonation in the bytownite mantle formed by exsolution after crystallization. The occurrence of micro-scale zoning in plagioclase indicates a minimum cooling rate of 0.0005 ºC/year during crystallization, assuming an initial temperature of 880 ºC, width of 50 μm and NaSi-CaAl interdiffusion under hydrous conditions. Assuming a formation temperature of ~675 ºC for the nano-scale exsolution texture as constrained by zircon crystallization temperatures, the retention of nano-scale zoning (~28 nm) requires a minimum cooling rate of 0.26 ºC/year. Given that this is significantly faster cooling than would occur in a magma chamber, this texture likely records the post-crystallization emplacement history.

Keywords: Atom probe tomography, plagioclase zonation, micro-scale and nano-scale, Black Mountain porphyry Cu deposit, Phillipines

INTRODUCTION

Textural and compositional zoning in plagioclase could be classified as micro-scale (10-100μm) and nano-scale (10-100 nm) according to the periodic width of zonation. Characterization of such zones can provide useful information on the crystallization environment (Stamatelopoulou-Seymour et al. 1990; Hattori and Sato 1996; Ginibre and Wörner 2007; Singer et al. 2016), with implications for the petrogenesis of host rocks (Haase et al. 1980; Allègre et al. 1981), metallogenesis of porphyry Cu deposits (Cao et al. 2014, 2018a, 2018b) and thermal history of related rocks (e.g., Grove et al. 1984; Liu and Yund 1992). However, the origin of micro- and nano-scale oscillatory zoning in plagioclase remains poorly understood, and the role of less well-constrained physical and chemical parameters (such as temperature, pressure, melt composition, H_2O and fO_2) and post-crystallization diffusion needs to be explored. In addition, the origin of both micro- and nano-scale zonation in the same plagioclase crystal is rarely studied (Grove et al. 1983).

The Baguio district (Philippines) is one of the world's premier mineral provinces, with more than 50 Moz of Au and 6 Mt of Cu (past production + resource; Malihan and Ruelo 2009) related to Pliocene-Pleistocene andesitic rocks (Cooke et al. 2011; Waters et al. 2011). The Black Mountain porphyry Cu-Au deposit is located in the center of the Baguio district and is closely related to the syn-mineralization diorite porphyry (2.98 to 2.83 Ma; Hollings et al. 2013). The porphyry contains widespread fresh, primary plagioclase phenocrysts with complex oscillatory zoning, providing the ideal natural laboratory in which to investigate magmatic processes linked to large scale mineralization.

Atom probe tomography (APT) can characterize previously inaccessible nano-scale compositional variations in a range of minerals and provide 3D images of atomic distribution for a range of geoscience applications (e.g., Gault et al. 2012; Kelly and Larson 2012; Valley et al. 2014; Fougerouse et al. 2016, 2018; Peterman et al. 2016; Piazolo et al. 2016; Reddy et al. 2016; White et al. 2017; Saxey et al. 2018). In this study, we have used electron microprobe (EMP), laser ablation inductively coupled plasma mass spectrometry (LA-ICPMS) and APT to characterize micro- and nano-scale elemental zonation in plagioclase from the syn-mineralization diorite porphyry at the Black Mountain porphyry Cu-Au deposit. The characteristics of micro- and nano-scale plagioclase zonation was used to provide insights into crystallization processes in the magma chamber and the thermal history of the deposit.

GEOLOGICAL SETTING AND PETROGRAPHY

The Baguio mineral district is located approximately 220 kilometers north of Manila (Philipines), at the southern end of the Luzon Central Cordillera. The geology and geochronology of the Baguio district were reviewed in detail by Waters et al. (2011) and Hollings et al. (2011). The Black Mountain porphyry Cu-Au deposit consists of two orebodies associated with the Black Mountain intrusive complex, and has a total resource of 65 Mt at 0.40 % Cu and 0.38 g/t Au (Malihan and Ruelo 2009). The description of intrusive phases and formation ages are given in Hollings et al. (2013). All these rocks show typical features of island arc magmatism (Hollings et al. 2013). Our previous works indicated complex crystallization processes, including repeated addition of mafic and felsic magmas to all the intrusive phases from the pre-mineralization diorite porphyry (~6.39 ± 0.49 Ma) to syn-mineralization diorite porphyry (2.98 ± 0.02 to 2.83 ± 0.23 Ma) (Hollings et al. 2013; Cao et al. 2018a, 2018b). Here, we focus on complex plagioclase phenocrysts from the relatively fresh syn-mineralization diorite porphyry.

Sample BA08GS030 from the diorite porphyry shows porphyritic textures with phenocrysts of plagioclase (~30 vol.%, 1.0 to 6.0 mm long) and amphibole (~16 vol.%, 0.5 to 4 mm long) in a groundmass of plagioclase (< 0.5 mm long), amphibole (< 0.3 mm long), biotite (< 0.3 mm long) and quartz (< 0.2 mm long) (Fig. 1a, 1b). Most euhedral plagioclase phenocrysts show well-developed oscillatory zoning, or complex zonation with patchy zones in the core. Tiny plagioclase crystals (<150 μm long) are rarely observed within amphibole phenocrysts. Primary amphibole crystals mainly occur as independent phenocrysts or are included in plagioclase phenocrysts (Fig. 1c), indicating that they formed slightly prior to, but mainly coeval with, plagioclase. Trace grains of apatite (60 to 200 μm) mainly occur in the groundmass with a few contained in plagioclase. Minor co-existing unzoned magnetite and ilmenite crystals are observed (more magnetite than ilmenite), indicating relatively oxidizing conditions. Tiny euhedral crystals of anhydrite (5×25 μm and 20×80 μm) were found contained in the patchy and oscillatory zones of plagioclase phenocrysts. In the groundmass, zircon is sparsely observed and quartz only occurs as small crystals. From these textural relations, a sequence of magmatic crystallization can be observed from amphibole ≈ plagioclase → apatite → Fe-Ti oxides ≈ zircon → quartz. The euhedral plagioclase crystal (3.0 × 5.4 mm) analyzed in this study has a patchy zone in the core which is eroded or replaced by Ca-rich zone in the mantle, and has oscillatory zonation in the rim (Fig. 1d). Given that the studied crystal shows similar features (patchy and oscillatory zoning) to the majority of plagioclase phenocrysts from other intrusive phases, it is considered representative and used to constrain formation processes. In order to investigate the nano-scale variations within zones, two specimens were prepared for atom probe tomography analysis from two regions of interest (Fig. 1d) including the Ca-rich mantle (APT 1) and oscillatory rim (APT 2).

ANALYTICAL METHODS

The major element compositions of plagioclase and amphibole were measured at the Institute of Geology and Geophysics, Chinese Academy of Sciences (IGGCAS) in Beijing, using a JEOL-JXA8100 EMP operated in wavelength dispersive spectrometer mode. The operating conditions were 15 kV accelerating voltage, 20 nA beam current and 3 μm spot size with counting times of 20 s for Na, K, Mg, Si, Mn, Al, Ca, Fe, Cr, Ti, F and Cl at their characteristic X-ray line. The following natural minerals and synthetic oxides were used for calibration: diopside (Ca, Mg and Si), rutile (Ti), jadeite (Al), hematite (Fe), synthetic MnO (Mn), albite (Na), orthoclase (K), chromite (Cr), tugtupite (Cl) and fluorite (F). All data were corrected using the atomic number-absorption-fluorescence procedure. X-ray maps for Ca and Na in the plagioclase crystal were performed in WDS mode using a CAMECA SX Five FE Electron Probe Microanalyzer at IGGCAS, with an accelerating voltage of 15 kV, a beam current of 250 nA, a 1.5 μm pixel size and dwell time of 20 ms. Plagioclase and amphibole major elemental compositions are presented in Supplementary Table A.1.

In situ trace element analysis of plagioclase in thick sections was carried out by LA-ICPMS on an Agilent 7700x quadrupole inductively coupled plasma mass spectrometer coupled to a Resonetics S-155-LR 193 nm excimer laser ablation system at the GeoHistory Facility in the John de Laeter Centre, Curtin University, Perth, Australia. Following a 30 s period of background analysis, plagioclase was ablated with a 33 μm beam for 30 s at a 5 Hz repetition rate and using a laser energy (measured at the sample surface) of 2.0 J/cm^2. The sample cell was flushed with ultra-high purity He (350 mL/min) and N_2 (3.6 mL/min). High-purity Ar was utilized as the carrier gas. NIST 610 was used as the primary standard with NIST 612 treated as a secondary standard. The internal reference isotope (^{29}Si) for plagioclase was determined from electron microprobe SiO_2 values. Data reduction and concentration calculations were performed using the Trace Elements data reduction scheme in Iolite (Paton et al. 2011). Based on analysis of secondary standard glasses, the accuracy of the trace element determinations was typically better than 4 % for most elements. *In situ* trace element analytical results for reference material and plagioclase are listed in Supplementary Table A.2.

Atom probe tomography analyses were performed on a Cameca LEAP 4000X HR at the Advanced Resource Characterization Facility housed in the John de Laeter Center at Curtin University. Atom probe tomography involves pulsed, laser-assisted field evaporation of atoms from the tip of a small needle-shaped specimen (Fig. 1d), coupled with time of flight mass spectrometry. Atoms liberated from the specimen tip are ionized and accelerated by an electric field to hit a position-sensitive detector. Using time-of-flight mass spectrometry, the time from laser pulse to ion detection yields the mass/charge ratio that is used to identify the ionic species (e.g., Miller and Forbes 2014). Unlike most ion sputtering techniques, all atoms in the sample are ionized and there is no significant fractionation of ionic species during the analysis. This leads to good counting statistics and reasonable precision without the need for reference materials to provide calibration of the data. Detection limits are typically at the ppm level, although this is dependent upon how the elements are distributed in the sample. Atom probe data are typically represented as reconstructions that show the 3D distribution of atoms in the specimen.

For atom probe tomography analysis, the specimens were extracted from the sample surface and prepared using a Tescan LYRA3 Focused Ion Beam Scanning

Electron Microscope (FIB-SEM) with a Ga^+ ion source, employing the standard lift-out technique (Thompson et al. 2007). The instrument was operated at an accelerating voltage of 30 kV during sample preparation and at 2 kV to remove the damaged layer created by the high-energy Ga ions. For APT analysis, the specimen base temperature was maintained at 60 K. An ultraviolet (λ= 355 nm) laser was focused on the specimen apex and pulsed at 200 kHz, with a pulse energy of 300 pJ. The detection rate was maintained at 0.01 atom/pulse for a total of 20 million atoms for each specimen (~3 h/specimen). The three dimensional information was recorded using a position-sensitive detector with the succession of detection events, and the chemical compositions determined using time-of-flight mass spectrometry. On the mass/charge spectra, peaks twice those of the background level were identified and ranged using the Cameca IVAS 3.6.10 processing software. In this study, concentrations are reported in atomic percent (atom %) for all major elements. Details of acquisition and reconstruction parameters are given in supplementary Table A.3 following the recommendations of Blum et al (2018).

RESULTS

Micro-scale plagioclase and amphibole mineral chemistry

Both the backscattered electron image (Fig. 2a) and Ca and Na X-ray maps (Fig. 2b, 2c) of the plagioclase phenocryst show distinct zonation including a patchy core with an eroded edge, Ca-rich mantle and an oscillatory zoned rim. EMP traverse shows oscillatory zoning for SiO_2, CaO, Al_2O_3, Na_2O and K_2O contents (wt%), and An $(100^*Ca/(Ca+Na+K)_{\text{in mole}})$ with an amplitude (ΔAn values) of 4 to 12 mol% in both the patchy core and the oscillatory zoned rim (Fig. 2). The zonation bands in the rim are 50 to 200 μm wide. The mantle zone has relatively low contents of SiO_2, Na_2O and K_2O (wt%), high CaO and Al_2O_3 (wt%), and high An but low Ab $(100*Na/(Ca+Na+K)_{in\ mole})$ and Or $(100*K/(Ca+Na+K)_{in\ mole})$ (Fig. 2). Similarly the mantle shows a zonation in trace elements including Fe, Mg, Ti, Ba, La, Ce and Pr (Fig. 3). Both the patchy core and oscillatory rim have similar abundances and patterns of oscillatory zonation for Fe, Mg, Ti, Sr, Ba, Pb, La, Ce and Pr (Fig. 3).

All analyzed amphibole, including grains contained in plagioclase and as phenocrysts and groundmass from BA08GS030 are calcic, containing >1.5 Ca atoms per fomula unit (a.p.f.u.; n = 50, Table A.1). All the amphibole grains are Mg-hornblende to tschermakite according to Leake et al. (1997) with Si (a.p.f.u.) values of 6.40 to 7.10, $Mg/(Mg+Fe^{2+})_{in\ mole}$ ratios of 0.65 to 0.87, $(Na+K)_A$ (a.p.f.u.) values of 0.06 to 0.42 and Ti (a.p.f.u.) values of 0.09 to 0.18. The grains contained in plagioclase and as large phenocryst show similar compositions with SiO_2 values of 43.7 to 44.9 wt%, Al_2O_3 values of 10.1 to 11.2 wt% and FeO values of 13.8 to 16.0 wt% (Table A.1). In contrast, the small crystal of amphibole (< 0.3 mm long) in the groundmass show higher contents of SiO_2 (47.6 to 49.5 wt%) and lower contents of Al_2O_3 (6.2 to 6.7 wt%) and FeO (12.5 to 13.4 wt%; Table A.1). The distinct compositions of amphibole probably indicate a different stage of formation.

Nano-scale plagioclase chemistry

The atom probe mass spectrum appears complex with the occurrence of single, double and triple charge state ionic species (Fig. 4). Of interest for this study, Ca was identified as Ca^{++} and Ca^{+}, whereas Na was observed as Na^{+}, NaO^{+} and Na_2O^{+}. We have used the total Ca and Na count numbers for each peak to calculate the composition of the nano-scale domains. Sr was identified at 88 Da (Mass/Charge ratio) for $^{88}Sr^{+}$, but no other Sr isotopes were observed above the background level.

Atom probe specimen 1 (APT 1), collected from the Ca-rich mantle zone, shows alternating 25 to 30 nm bands of different compositions with Al-, Ca-rich domains and Si-, Na-rich zones (Fig. 5). A 1D concentration profile across several of the bands shows a $Ca/(Ca+Na)_{atom\ \%}$ amplitude of about 10 and a sharp (<2 nm) transition between domains (Fig. 5). The $Ca/(Ca+Na)_{atom\ \%}$ ratio for the whole sample determined by atom probe is 79.9, similar to the EMP results (79.5 to 79.7).

Atom probe specimen 2 (APT 2), collected from the oscillatory rim, shows a homogeneous distribution of all ionic species, including Ca, Na, Al and Si (Fig. 6). The $Ca/(Ca+Na)_{atom\ \%}$ ratio of specimen 2 determined by atom probe (55.0) is slightly higher than that from the EMP (43.0 to 43.8), likely reflecting variations in bulk composition resulting from the different analytical volumes analyzed using two different techniques.

DISCUSSION

Plagioclase crystallization conditions

Assuming a similar crystallization sequence for plagioclase and amphibole, we can estimate the formation conditions of plagioclase using amphibole thermobarometry and oxybarometers. Based on a compilation of published experimental results, Ridolfi et al. (2010) proposed that amphibole chemistry in subduction-related calc-alkaline rocks can be used to estimate crystallization temperature and oxidation state. The validity of this method was confirmed by Erdmann et al. (2014) by comparing experimental and calculated results. In addition, pressure can be estimated using the Al-in-hornblende geobarometer (Schmidt 1992).

Using the method of Ridolfi et al. (2010), our results show a relatively restricted formation temperature (865 to 895 ºC; mean = 878 ± 10 ºC, 1σ, n = 16) for amphibole inclusions in plagioclase and for amphibole phenocrysts (864 to 893 ºC; mean = 878 ± 9 ºC, 1σ, n = 21; Fig. 7) with 1σ uncertainty of 22 ºC. These values are higher than the formation temperature of groundmass amphibole crystals (769 to 800 ºC, n = 13) with 1σ uncertainty of 22 ºC, which are in turn higher than those for accessory minerals including zircon and co-existing magnetite-ilmenite in the groundmass (700 to 750 ºC; Cao et al. 2018a). The calculated formation temperatures indicate early crystallization of amphibole phenocrysts, followed by groundmass amphibole and late accessory minerals, consistent with the crystallization sequence indicated by textural relationships.

The Al-in-hornblende geobarometer yielded higher crystallization pressures (from 5.3 to 6.2 kbar with a mean of 5.8 kbar) for the early stage of amphibole compared with groundmass amphibole (1.9 to 2.4 kbar, with a mean of 2.2 kbar, Fig. 7) with a precision of ± 0.6 kbar according to Schmidt (1992). The distinct crystallization temperature and pressure indicate two different formation environments for these texturally distinct forms of amphibole.

The amphibole oxybarometer of Ridolfi et al. (2010) indicated an oxidation state of NNO+0.6 to NNO+1.1 (mean = NNO+0.9; Fig. 7c) for amphibole phenocrysts, and fO_2 values of NNO+0.6 to NNO+1.9 (mean = NNO+1.3; Fig. 7c) for groundmass amphibole. These results are consistent with the occurrence of anhydrite in plagioclase phenocrysts (Cao et al. 2018a) which requires an oxygen fugacity of ≥NNO+1. The values of NNO+0.6 to NNO+1.9 obtained on groundmass amphibole are similar but slightly lower than that those yielded by late crystallized co-existing magnetite-ilmenite pairs (Cao et al. 2018a) (NNO+1.9 to NNO+2.4), indicating a subtle increase in oxygen fugacity from the early to late magmatic stages. Considering the similar formation sequence for phenocrysts of amphibole and plagioclase indicated by the textural relations, the crystallization conditions for amphibole phenocrysts (T = 865 to 895 ºC, P = 5.3 to 6.2 kbar, fO_2 = NNO+0.6 to NNO+1.1) are assumed to be the same as for the plagioclase phenocrysts.

Micro-scale zonations in plagioclase

Two different models have been proposed to account for micro-scale oscillatory zoning in plagioclase: (1) Variations of physiochemical conditions (e.g., T, P, fO_2, H_2O and melt composition) (e.g., Stamatelopoulou-Seymour et al. 1990; Hattori and Sato 1996; Ginibre and Wörner 2007); and (2) Changes in internal crystal growth mechanisms due to the interplay between interface kinetics and elemental diffusion in the melt (e.g., Sibley et al. 1976; Haase et al. 1980; Allègre et al. 1981; Ortoleva 1990; L'Heureux et al. 1994). During crystallization of plagioclase, variations in a range of parameters (e.g., temperature, pressure, H_2O content, oxygen fugacity and melt compositions) can change its composition and have been suggested to cause micro-scale oscillatory zoning (e.g., Stamatelopoulou-Seymour et al. 1990; Hattori and Sato 1996). Variations in pressure have a relatively weak effect on the chemistry of crystallizing plagioclase when compared to temperature, H_2O content and melt compositions (Housh and Luhr 1991; Panjasawatwong et al. 1995; Lange et al. 2009). It is worth noting that the Al-in-hornblende geobarometer records limited variations of pressure (6.6 to 5.1 kbar), indicating a relatively stable pressure conditions in the magma chamber (~5.8 kbar) during plagioclase crystallization. A gradual increase of 4.5 mol% An in plagioclase could result from a pressure decrease from 6.6 to 5.1 kbar according to Ustunisik et al. (2014), whereas repeated variations of An in oscillatory zoning of plagioclase (Fig. 2) cannot be generated in a relatively stable magma chamber.

Changes in oxygen fugacity can affect the Fe, Ce, Eu, V and Cr contents of plagioclase but has no obvious effect on other elements (Phinney 1992; Wilke and Behrens 1999; Aigner-Torres et al. 2007). The relatively restricted range of oxygen fugacity values (NNO+0.6 to NNO+1.1; Fig. 7c) obtained on amphibole phenocrysts suggests there would be only limited impact of fO_2 variation on plagioclase-melt partition coefficients according to the results of Wilke and Behrens (1999). Limited variation in Fe content in the patchy core zone and oscillatory zoned rim also suggests limited variations in fO_2, consistent with the results from the amphibole oxybarometer (Fig. 7c). For the Ca-rich mantle zone, obvious correlation between Fe and other elements (Ca, Na, K, Mg, Ti and Ba; Fig. 3) further eliminates oxygen fugacity as the critical factor controlling composition in the mantle zone of the crystal.

Variations in H_2O content caused by an influx of external fluids or degassing of the magma chamber will affect albite–anorthite binary loops and, thus, the An values of crystallizing plagioclase. This, in turn, controls the partition coefficient of other trace elements (e.g., Sr, Ba; Blundy and Shimizu 1991; Blundy and Wood 1991; Bindeman et al. 1998). The occurrence of amphibole inclusions in both the oscillatory and patchy zones of the plagioclase phenocrysts (Fig. 2) indicates relatively high H_2O contents during plagioclase formation and is consistent with the widespread presence of amphibole phenocrysts. Using the method of Lange et al. (2009), and assuming that the whole rock composition represents the melt composition and that the mean An value of plagioclase from both core and rim represents the value of plagioclase, we can estimate the H_2O content of the melt. The result shows ~4.0 wt% H_2O for the melt, indicating relatively high H_2O contents during plagioclase formation. Although increased H_2O contents in the magma likely occurred from the early to late stage (discussed later in implications), the oscillatory An variations in early stage crystallized plagioclase phenocryst cannot be generated by increasing H_2O. Thus, limited variations of H_2O content are likely the case for our analyzed plagioclase, and the effect of H_2O variations on plagioclase chemistry is minor.

Melt temperature has a significant effect on plagioclase compositions with higher temperatures favoring higher anorthite contents (Housh and Luhr 1991; Lange et al. 2009). Given similar crystallization conditions for the amphibole inclusions and host plagioclase, small variations in formation temperature (865° to 895 °C) for amphibole contained in the oscillatory rim zone implies limited temperature variations were experienced by the host plagioclase. In contrast, the patchy core, with an obvious corroded edge (Fig. 2), was probably heated by a higher temperature mafic magma, consistent with the formation of bytownite in the mantle zone.

Melt composition exerts a strong control on plagioclase chemistry with anorthite to bytownite forming in mafic rocks and labradorite to andesine compositions in andesitic rocks (Panjasawatwong et al. 1995). The bytownite mantle zone of the studied plagioclase crystal ($An_{79–71}$ mol%) likely formed from a relatively mafic magma, whereas both the patchy zone ($An_{47–41}$ mol%) and oscillatory rim ($An_{51–39}$ mol%) consistently indicate formation of plagioclase in an andesitic magma. The coupled increase in Fe, Mg and Ti, and decrease in Sr, Ba, Pb, La, Ce and Pr within the bytownite mantle (Fig. 3) also suggest that it crystallized from a relatively more primitive melt. Although crystal growth rate will affect the elemental composition of plagioclase, the abrupt compositional variations in the bytownite mantle could not have been caused by changes in growth rate. Thus, the bytownite composition of the mantle zone indicates the addition of a relative high temperature mafic melt into the andesitic magma chamber, consistent with previous amphibole and plagioclase studies (Hollings et al. 2013; Cao et al. 2018a). The compositional similarity of oscillatory zones in both the patchy core and oscillatory rim (Figs. 2, 3) suggests that there was pre-existing oscillatory zonation in the core, prior to injection of mafic magma which corroded the edge of the crystal and generated the patchy texture.

In summary, our results indicate that plagioclase formed in an andesitic magma chamber under stable pressure (~5.8 kbar), temperature (865 to 895 ºC), oxygen fugacity (NNO+0.6 to NNO+1.1) and hydration conditions (all according to analyses of co-precipitated amphibole). Thus, the micro-scale oscillatory zoning was not principally controlled by externally imposed variations in physiochemical conditions (e.g., T, P, fO_2, H_2O and melt composition) recorded at other locations (e.g., Stamatelopoulou-Seymour et al. 1990; Hattori and Sato 1996; Ginibre and Wörner 2007).

Limited An variation in both the patchy core ($An_{47–41}$ mol%) and oscillatory rim ($An_{51–39}$ mol%) suggests that internal crystal growth mechanisms had an influence on crystal composition (e.g., Sibley et al. 1976; Haase et al. 1980; Allègre et al. 1981; Ortoleva 1990; L'Heureux et al. 1994). Internal crystal growth mechanisms are impacted by various factors including growth rate, elemental diffusion and elemental partitioning, none of which are well constrained. However, assuming a lack of elemental diffusion and constant elemental partitioning, we can qualitatively compare the trace element cargo in plagioclase at different growth rate. Considering the obvious higher contents of Fe, Mg, Ti, La, Ce and Pr in co-precipitated amphibole compared to plagioclase (Cao et al. 2018a), and thus significant effect that amphibole crystallization had on plagioclase, we can only estimate the variations of Sr, Ba and Pb under different growth rate. Assuming that; (1) plagioclase/andesite partition coefficient values are $D_{Sr} = 2.7$, $D_{Ba} = 0.38$ and $D_{Pb} = 1.07$, obtained previously on calc-alkaline andesitic rocks (Dunn and Sen 1994); (2) melt values were $C_{Sr\ in\ melt} = 578.7$ ppm, $C_{Ba\ in\ melt} = 189$ ppm and $C_{Pb\ in\ melt} = 1.03$ ppm as represented by the BA08GS030 bulk compositions (Hollings et al. 2013); and (3) the proportion of crystallized plagioclase to melt was f = 0.05 and f = 0.2, corresponding to different growth rates, we can calculate the contents of Sr, Ba and Pb in plagioclase ($C_{\mathrm{Sr\ in\ plagioclase}}$, $C_{\mathrm{Ba\ in\ plagioclase}}$, $C_{\mathrm{Pb\ in\ plagioclase}}$). The results show $C_{\mathrm{Sr\ in\ plagioclase}}$ = 1440 ppm, $C_{\mathrm{Ba\ in\ plagioclase}}$ = 74 ppm and $C_{\mathrm{Pb\ in\ plagioclase}}$ = 1.1 ppm for f = 0.05, and $C_{\mathrm{Sr\ in\ plagioclase}}$ = 1166 ppm, $C_{\mathrm{Ba\ in\ plagioclase}}$ = 82 ppm and $C_{\mathrm{Pb\ in\ plagioclase}}$ = 1.1 ppm for f = 0.2. The decrease in Sr content in plagioclase from $C_{\mathrm{Sr\ in\ plagioclase}}$ = 1440 ppm to $C_{\mathrm{Sr\ in\ plagioclase}}$ = 1166 ppm with increased growth rate is consistent with our measured results (Fig. 3d), supporting a growth rate control on composition. In addition, the slight increase for Ba in the oscillatory rim (Fig. 3e) show similar trend with our calculation from 74 ppm to 82 ppm. The different contents of Ba and Pb in plagioclase may be related to the difference in partition coefficients and the effects of other co-precipitated minerals (such as amphibole). Thus, we propose that the micro-scale oscillatory zoning in our sample was probably generated by internal crystal growth mechanisms.

The overall plagioclase crystal provides evidence of three distinct processes, from core to rim, including: (1) a patchy core derived by heating of an existing oscillatory zoned core; (2) Ca-rich mantle crystallized during injection of a high temperature relatively mafic melt; and (3) micro-scale oscillatory zoned rim which grew under relatively stable conditions in an andesitic magma chamber.

Nano-scale zonations in plagioclase

Due to their low spatial resolution, many techniques (including EMP, LA-ICPMS and secondary ion mass spectrometry) cannot recognize and/or accurately measure sub-micron compositional features in plagioclase. The profile for specimen APT 1 from the bytownite mantle shows alternating Al-, Ca-rich and Si-, Na-rich zones with zone widths of 25 to 30 nm. These domains are characterized by Ca/(Ca+Na)$_{\text{atom \%}}$ variations of about 10, which is similar to the amplitude of micro-scale oscillatory zoning in the rim revealed by EMP (Fig. 2). Two distinct models can explain the 25 to 30 nm compositional variations observed in specimen APT 1, including nano-scale oscillatory zoning during crystallization and exsolution after crystallization.

If the An nano-scale oscillatory zoning is the result of crystallization processes alone, the interdiffusivity of CaAl-NaSi in the crystal should have been slow enough not to be homogenized during crystallization. To test this hypothesis, we have used the analytical formulation of the diffusion equation of Crank (1975). According to Crank (1975), when the dimensionless parameter Dt/l^2 (where D is the diffusion coefficient, t is the time, l is half of the zonation width) is 0.5, the compositional difference between zones is reduced to 0.01 and homogenization is essentially complete. The amphibole inclusions in plagioclase indicate a hydrous environment and crystallization temperature of ~880 ºC, and by proxy, we assume the same temperature for plagioclase crystallization. According to the CaAl-NaSi interdiffusion coefficient of Liu and Yund (1992), under hydrous conditions, at 880 ºC, and with a zone width of ~30 nm, the uniform diffusion timescale required for homogenization of CaAl-NaSi zonation is only ~0.02 years (7 days).

Although the processes of magma cooling, upward emplacement and water exsolution may affect crystal growth rate to some extent (Brugger and Hammer 2010), the most common growth rate for plagioclase in basaltic or andesitic magmas is in the range of 10^{-6} to 10^{-8} mm/s (e.g., Salisbury et al. 2008; Brugger and Hammer 2010; Pappalardo and Mastrolorenzo 2010). The thickness of the crystal zone from bytownite mantle to oscillatory rim is ~1.25 mm, requiring a crystallization timescale of 0.04 to 4.0 years. This crystallization timescale is 2 to 200 times longer than the uniform diffusion timescale of homogenization for CaAl-NaSi zonation, indicating that the nano-scale features observed in the bytownite mantle did not form during crystallization.

Numerous transmission electron microscopy studies have revealed nano-scale exsolution textures in plagioclase crystals with bytownite compositions (Huttenlocher exsolution as first observed by Huttenlocher 1942; Grove 1977; Kitamura and Morimoto 1977; Wenk and Nakajima 1980; Grove et al. 1984; Liu and Yund 1992). Huttenlocher exsolution (also called Huttenlocher intergrowth) occurs in calcic plagioclases with bulk compositions from about An_{67} mol% to An_{90} mol% (Smith and Brown 1974). The periodicity of exsolution lamellae decreases with increasing An content (~85 nm at An_{74-75} mol%, 60 nm at An_{76-79} mol%, 40 nm at An_{81} mol%, 20 nm at An_{82} mol%, 13 nm at An_{85} mol%, and is barely visible at An_{89} mol%; Grove 1977). Figure 5 shows an obvious zonation in Al, Ca, Na and Si in atom %. The bulk compositions of specimen APT 1 shows a $Ca/(Ca+Na+K)_{atom\ \%}$ ratio of 80 which is consistent with EMP results (An_{79-80} mol%; Fig. 1). In addition, the 25 to 30 nm width of the Al-, Ca-rich and Si-, Na-rich zones and periodicity of ~55 nm (Fig. 5) are consistent with the wavelength of exsolution lamellae for bulk An contents of An_{76-79} mol% (60 nm) and An_{81} mol% (40 nm) (Grove 1977). The exact compositions of the two products of the exsolution are probably related to the bulk composition and the cooling history, and thus are difficult to predict. Grove et al. (1983) ascribed the $I\bar{1} \leftrightarrow P\bar{1}$ transformation as the mechanism of Huttenlocher exsolution. Furthermore, the absence of elemental zoning in the oscillatory rim (An_{42} mol%) of specimen APT 2 ($Ca/(Ca+Na)_{atom\ \%} = 55.0$) suggests exsolution is less likely to occur for intermediate plagioclase after crystallization, although the composition of An_{42} mol% or $Ca/(Ca+Na)_{atom\ \%} = 55.0$ was located in an area of Bøggild intergrowth (occurs in plagioclase with bulk composition from An_{43} mol% to An_{58} mol% and forms the lamellae ranging near An_{39-48} mol% and An_{53-64} mol%; Smith and Brown 1974). All the above evidence consistently implies that the nano-scale zonation in the bytownite mantle was probably generated by Huttenlocher exsolution after crystallization.

IMPLICATIONS

The presence of compositional and oscillatory zoning suggests a faster cooling rate (V) for this crystal than for homogeneous crystals. Assuming that homogenization occurred in the crystals, the cooling rate can be expressed as $V = RD_0T_0^2/(0.5Ql^2)\exp(-Q/(RT_0))$ which represents the minimum cooling rate required to retain the oscillatory zoning, as given by Grove et al. (1984) based on the calculation of Walker et al. (1977), where l is half the zonation width, T_0 is initial temperature in Kelvin after isolation from the melt, D_0 and Q are the Arrhenius parameters for diffusion data, and R is the universal gas constant. Adopting the NaSi-CaAl interdiffusion of Liu and Yund (1992) and initial temperature of 880 ºC estimated from amphibole thermometry (Ridolfi et al., 2010), the minimum cooling rate is

0.0005 ºC/year where $l \approx 25$ μm, $D_0 = 1.1 \times 10^{-5}$ m^2/s, Q = 371 KJ/mol.

A compilation of previously published zircon chemical-abrasion, isotope dilution thermal ionization mass spectrometry ^{206}Pb/^{238}Pb ages indicates a long period of zircon crystallization for the syn-mineralization diorite porphyry at Black Mountain from 3.01 to 2.82 Ma (Hollings et al. 2013), which implies a slow cooling rate in the magma chamber (Fig. 8). This is consistent with a long-lived and hot felsic magma chamber under the Black Mountain deposit indicated by similarity of crystallization temperature and pressures from 6.39 ± 0.49 Ma to 2.83 ± 0.23 Ma (Cao et al. 2018a). If we take the age interval of 0.19 m.y. (i.e. 3.01–2.82 Ma) and a cooling temperature of 110 ºC from 780 to 670 ºC during this interval, calculated from Cao et al. (2018a), we can estimate an average cooling rate of (780-670)/[(3.01-2.82)*1000000] = 0.0006 ºC/year which is comparable to the minimum cooling rate of 0.0005 ºC/year required to retain oscillatory zoning. Such a slow cooling rate is supported by: 1) the deep crustal level for the magma chamber indicated from the amphibole barometer (~5.8 kbar), and 2) the addition of high temperature mafic magma to the chamber as indicated by the Ca-rich mantle zone and eroded core of the plagioclase crystal (Fig. 2).

Although there is debate regarding the mechanism and formation temperature of Huttenlocher exsolution (Smith and Ribbe 1969; Grove 1977; Wenk and Nakajima 1980), the preservation of 25 to 30 nm compositional variations in the analyzed sample provides some valuable constraints on the temperature of Huttenlocher exsolution. If the formation temperature of nano-scale zonation occurred at ≥700 ºC representing the minimum formation temperature of late stage mineral phases (Fig. 7), it would only take ~23.4 years to homogenize nano-scale zonation according to the CaAl-NaSi interdiffusion coefficient of Liu and Yund (1992). Based on the average cooling rate revealed by zircon (0.0006 ºC/year), it would take ~34,500 years to cool from 700 to 680 ºC. This indicates that the formation of Huttenlocher exsolution occurred below 700 ºC. If we exclude the lowest zircon crystallization temperature (663ºC), all 83 remaining zircon grains from the diorite porphyries show formation temperatures of 670 to 780 ºC (Fig. 9; Cao et al. 2018a). This implies andesitic magma consolidation at ~670 ºC and upwards emplacement of andesitic magma from a deep magma chamber to a shallow level. After emplacement, the diorite porphyry should have cooled rapidly due to significant heat transfer to the wall-rock at shallow levels. Huttenlocher exsolution in bytownite is less likely to occur under fast cooling conditions. Thus, the Huttenlocher exsolution was probably generated at temperatures of 670 to 700 ºC at a slow cooling rate, just before or coeval with upwards emplacement, leaving the plagioclase only a very short time to undergo diffusion and retain nano-scale zoning. This value is consistent with the formation temperature of ~675 ºC proposed by Grove et al. (1983).

Taking ~675 ºC as the formation temperature of Huttenlocher exsolution, we can also estimate the minimum cooling rate required to retain nano-scale compositional variations. A minimum cooling rate of 0.26 ºC/year is needed when l = 14 nm, at an initial temperature of 675 ºC and using the NaSi-CaAl interdiffusion parameters of Liu and Yund (1992). A faster minimum cooling rate of 0.26 ºC/year below 675 ºC compared to a rate of 0.0005 ºC/year above 675 ºC is consistent with the emplacement of the diorite porphyry at a shallow level (Fig. 9).

Many studies have indicated that the addition of mafic magma introduces abundant Cu to porphyry systems (Mathur et al. 2000; Hattori and Keith 2001; Halter et al. 2005; Hollings et al. 2013; Cao et al. 2014, 2018a, 2018b; Blundy et al. 2015). The occurrence of bytownite in the mantle zone of the plagioclase crystal and the corroded core texture indicate the addition of a high temperature mafic magma. The common occurrence of rounded or elongated sulfide inclusions and higher contents of Cu in the megacrystic amphibole of coeval mafic dikes (2.81 ± 0.15 Ma), compared to the amphibole in syn-mineralization diorite porphyries, indicates highly enriched Cu characteristics for the coeval mafic magma (Cao et al. 2018a). In addition, the reversely zoned amphibole in syn-mineralization diorite porphyry shows obvious increases in Cu from core to rim, indicating much more enriched Cu for the injected mafic magma (Cao et al. 2018b). Thus, mantle-derived mafic magma likely played an important role in the petrogenesis of syn-mineralization andesitic rocks and provided some degree of ore-forming components (such as Cu) to the porphyry systems.

Our detailed investigation of a complex plagioclase phenocryst with distinct zonations reveals considerable information regarding crystallization processes in a deep magma chamber, and also preservations of its thermal history. These results have implications for petrogenesis (mafic and felsic magma mixing), metallogenesis (mafic magma-derived ore-forming components) and our understanding of cooling history of porphyry deposits (slow cooling in the magma chamber and fast cooling at the emplacement level). In addition, this study shows that there is wide scope for APT to be applied to the investigation of previously unresolvable nano-scale compositional variations in plagioclase and potentially other minerals.

ACKNOWLEDGMENTS

We thank Gabe Sweet and Mike Baker for sample collection, Anne Hammond and Kristi Tavener of Lakehead for sample preparation, Qian Mao for their assistance with EMP and X-ray map analysis at IGGCAS, Andrew Putnis of Curtin University for discussion on nano-scale zoning in plagioclase. This work was supported by National Key Research and Development Plan (2017YFC0601306), National Natural Sciences Foundation of China (41672090) and Youth Innovation Promotion Association CAS (2018086) to Mingjian Cao. The John de Laeter Centre (JdLC), Curtin University is thanked for access and technical support. GeoHistory Facility instruments in the JdLC, Curtin University were funded via an Australian Geophysical Observing System grant provided to AuScope Pty Ltd. by the AQ44 Australian Education Investment Fund program. The Australian Resource Characterisation Facility (ARCF) in the JdLC, under the auspices of the National Resource Sciences Precinct (NRSP) – a collaboration between CSIRO, Curtin University and The University of Western Australia – is supported by the Science and Industry Endowment Fund (SIEF RI13-01).

REFERENCES CITED

Aigner-Torres, M., Blundy, J., Ulmer, P., and Pettke, T. (2007) Laser ablation ICPMS study of trace element partitioning between plagioclase and basaltic melts: an experimental approach. Contributions to Mineralogy and Petrology, 153, 647–667.

Allègre, C. J., Provost, A., and Jaupart, C. (1981) Oscillatory zoning: a pathological case of crystal growth. Nature, 294, 223–228.

Bindeman, I.N., Davis, A.M., and Drake, M.J. (1998) Ion microprobe study of plagioclase-basalt partition experiments at natural concentration levels of trace elements. Geochimica et Cosmochimica Acta, 62, 1175–1193.

Blum, T.B., Darling, J.R., Kelly, T.F., Larson, D.J., Moser, D.E., Perez-Huerta, A., Prosa, T.J., Reddy, S.M., Reinhard, D.A., and Saxey, D.W. (2017) Best practices for reporting atom probe analysis of geological materials. In D.E. Moser, F. Corfu, J.R. Darling, S.M. Reddy, and K. Tait, Eds., Microstructural geochronology: Planetary records down to atom scale, p. 369-373. Wiley, Hoboken, New Jersey.

Blundy, J.D., and Shimizu, N. (1991) Trace element evidence for plagioclase recycling in calc-alkaline magmas. Earth and Planetary Science Letters, 102, 178–197.

Blundy, J.D., and Wood, B.J. (1991) Crystal-chemical controls on the partitioning of Sr and Ba between plagioclase feldspar, silicate melts, and hydrothermal solutions. Geochimica et Cosmochimica Acta, 55, 193–209.

Blundy, J., Mavrogenes, J., Tattitch, B., Sparks, S., and Gilmer, A. (2015) Generation of porphyry copper deposits by gas-brine reaction in volcanic arcs. Nature Geoscience, 8, 235–240.

Brandeis, G., Jaupart, C., and Allègre, C.J. (1984) Nucleation, crystal $owth and the thermal regime of cooling magmas. Journal of Geophysical Research, 89, l0l6l–10177.

Brugger, C.R., and Hammer, J.E. (2010) Crystal size distribution analysis of plagioclase in experimentally decompressed hydrous rhyodacite magma. Earth and Planetary Science Letters, 300, 246–254.

Cao, M.J., Qin, K.Z., Li, G.M., Yang, Y.H., Evans, N.J., Zhang, R., and Jin, L.Y. (2014) Magmatic process recorded in plagioclase at the Baogutu reduced porphyry Cu deposit, western Junggar, NW-China. Journal of Asian Earth Sciences, 82, 136–150.

Cao, M.J., Hollings, P., Cooke, D.R., Evans, N.J., McInnes, B.I.A., Qin, K.Z., Li, G.M., Sweet, G., and Baker, M. (2018a) Physicochemical processes in the magma chamber under the Black Mountain porphyry Cu-Au deposit (Philippines): Insights from mineral chemistry and implications for mineralization. Economic Geology, 113, 63–82.

Cao, M.J., Evans, N.J., Hollings, P., Cooke, D.R., McInnes, B.I.A., Qin, K.Z., Li, G.M. (2018b) Zonations of various phenocrysts in porphyry related rocks of the Baguio District, Philippines: Evidence for magmatic and metallogenic processes. Journal of Petrology, 59, 825–848.

Cooke, D.R., Deyell, C.L., Waters, P.J., Gonzales, R.I., and Zaw, K. (2011) Evidence for magmatic-hydrothermal fluids and ore-forming processes in epithermal and porphyry deposits of the Baguio district, Philippines. Economic Geology, 106, 1399–1424.

Crank J. (1975) The mathematics of diffusion, 2nd ed., 145 p. Oxford University Press, London.

Dunn, T., and Sen, C. (1994) Mineral/matrix partition coefficients for orthopyroxene, plagioclase, and olivine in basaltic to andesitic systems: A combined analytical and experimental study. Geochimica et Cosmochimica Acta, 58, 717–733.

Erdmann, S., Martel, C., Pichavant, M., and Kushnir, A. (2014) Amphibole as an archivist of magmatic crystallization conditions: problems, potential, and implications for inferring magma storage prior to the paroxysmal 2010 eruption of Mount Merapi, Indonesia. Contributions to Mineralogy and Petrology, 167, 1–23.

Ferry, J.M., and Watson, E.B. (2007) New thermodynamic models and revised calibrations for the Ti-in-zircon and Zr-in-rutile thermometers. Contributions to Mineralogy and Petrology, 154, 429–437.

Fougerouse, D., Reddy, S.M., Saxey, D.W., Rickard, W.D., Van Riessen, A., and Micklethwaite, S. (2016) Nanoscale gold clusters in arsenopyrite controlled by growth rate not concentration: Evidence from atom probe microscopy. American Mineralogist, 101, 1916–1919.

Fougerouse, D., Reddy, S.M., Saxey, D.W., Erickson, T.M., Kirkland, C.L., Rickard, W.D.A., Seydoux-Guillaume, A.M., Clark, C., and Buick, I.S. (2018) Nanoscale distribution of Pb in monazite revealed by atom probe microscopy. Chemical Geology, 479, 251–258.

Gault, B., Moody, M.P., Cairney, J.M., and Ringer, S.P. (2012) Atom probe microscopy, 396 p. Springer, New York.

Ginibre, C., and Wörner, G. (2007) Variable parent magmas and recharge regimes of the Parinacota magma system (N. Chile) revealed by Fe, Mg and Sr zoning in plagioclase. Lithos, 98, 118–140.

Grove, T.L. (1977) Structural characterization of labradorite-bytownite plagioclase from volcanic, plutonic and metamorphic environments. Contributions to Mineralogy and Petrology, 64, 273–302.

Grove, T.L., Ferry, J.M., and Spear, F.S. (1983) Phase transitions and decomposition relations in calcic plagioclase. American Mineralogist, 68, 41–59.

Grove, T.L., Baker, M.B., and Kinzler, R.J. (1984) Coupled CaAl-NaSi diffusion in plagioclase feldspar: Experiments and applications to cooling rate speedometry. Geochimica et Cosmochimica Acta, 48, 2113–2121.

Haase, C., Chadam, J., Feinn, D., and Ortoleva, P. (1980) Oscillatory zoning in plagioclase feldspar. Science, 209, 272–274.

Halter, W.E., Heinrich, C.A., and Pettke, T. (2005) Magma evolution and the formation of porphyry Cu–Au ore fluids: evidence from silicate and sulfide melt inclusions. Mineralium Deposita, 39, 845–863.

Hattori, K., and Sato, H. (1996) Magma evolution recorded in plagioclase zoning in 1991 Pinatubo eruption products. American Mineralogist, 81, 982–994.

Hattori, K., and Keith, J. (2001) Contribution of mafic melt to porphyry copper mineralization: evidence from Mount Pinatubo, Philippines, and Bingham Canyon, Utah, USA. Mineralium Deposita, 36, 799–806.

Hollings, P., Cooke, D.R., Waters, P.J., and Cousens, B. (2011) Igneous geochemistry of mineralized rocks of the Baguio district, Philippines: Implications for tectonic evolution and the genesis of porphyry-style mineralization. Economic Geology 106, 1317–1333.

Hollings, P., Sweet, G., Baker, M., Cooke, D., and Fiedman, R. (2013) Tectonomagmatic controls on porphyry mineralization: Geochemical evidence from the Black Mountain porphyry system, Philippines. SEG Special Publication, 17, 301–335.

Housh, T.B., and Luhr, J.F. (1991) Plagioclase-melt equilibria in hydrous systems. American Mineralogist, 76, 477–492.

Huttenlocher, H. (1942) Beiträge zur Petrographie des Gesteinzuges Ivrea Verbano I. Allgemeines. Die gabbroiden Gesteinen von Anzola. Schweizerische mineralogische und petrographische mitteilungen, 22, 326–366.

Kelly, T.F., and Larson, D.J. (2012) Atom probe tomography 2012. Annual Review of Materials Research, 42, 1–31.

Kitamura, M., and Morimoto, N. (1977) The superstructure of plagioclase feldspars.

Physics and Chemistry of Minerals, 1, 199–212.

Lange, R.A., Frey, H.M., and Hector, J. (2009) A thermodynamic model for the plagioclase-liquid hygrometer/thermometer. American Mineralogist, 94, 494–506.

Leake, B.E., Woolet, A.R., Arps, C.E.S., Birch, W.D., Gilbert, M.C., Grice, J.D., Hawthorne, F.C., Kato, A., Kisch, H.J., and Krivovichev, E.A. (1997). Nomenclature of amphiboles: re-port of the subcommittee on amphiboles of the International Mineralogical Association, Commission on New Minerals and Mineral Names. The Canadian Mineralogist, 35, 219–246.

Liu, M., and Yund, R.A. (1992) NaSi-CaAl interdiffusion in plagioclase. American Mineralogist, 77, 275–283.

L'Heureux, I., and Fowler, A.D. (1994) A nonlinear dynamical model of oscillatory zoning in plagioclase. American Mineralogist, 79, 885–891.

Mathur, R., Ruiz, J., and Munizaga, F. (2000) Relationship between copper tonnage of Chilean base-metal porphyry deposits and Os isotope ratios. Geology, 28, 555–558.

Malihan, T., and Ruelo, N. (2009) The Baguio mineral district, a giant multi-episodic clustered copper gold system [Online]. Available: http://rwg-tag.bravehost.com/Conferences/Surigao/Presentations/jun09-13h30-ruelo%20and%20malihan.pdf).

Miller, M.K., and Forbes, R.G. (2014) Atom-probe tomography: The local electrode atom probe, 423 p. Springer, New York.

Ortoleva, P.J. (1990) Role of attachment kinetic feedback in the oscillatory zoning of crystals grown from melts. Earth Science Reviews, 29, 3–8.

Panjasawatwong, Y., Danyushevsky, L., Crawford, A., and Harris, K. (1995) An experimental study of the effects of melt composition on plagioclase-melt equilibria at 5 and 10 kbar: implications for the origin of magmatic high-An plagioclase. Contributions to Mineralogy and Petrology, 118, 420–432.

Pappalardo, L., and Mastrolorenzo, G. (2010) Short residence times for alkaline Vesuvius magmas in a multi-depth supply system: Evidence from geochemical and textural studies. Earth and Planetary Science Letters, 296, 133–143.

Paton, C., Hellstrom, J., Paul, B., Woodhead, J., and Hergt, J. (2011) Iolite: Freeware for the visualisation and processing of mass spectrometric data. Journal of Analytical Atomic Spectrometry, 26, 2508–2518.

Peterman, E.M., Reddy, S.M., Saxey, D.W., Snoeyenbos, D.R., Rickard, W.D., Fougerouse, D., and Kylander-Clark, A.R. (2016) Nanogeochronology of discordant zircon measured by atom probe microscopy of Pb-enriched dislocation loops. Science Advances, 2, e1601318.

Phinney, W.C. (1992) Partition coefficients for iron between plagioclase and basalt as a function of oxygen fugacity: Implications for Archean and lunar anorthosites. Geochimica et Cosmochimica Acta, 56, 1885–1895.

Piazolo, S., Fontaine, A.L, Trimby, P., Harley, S., Yang, L., Armstrong, R., and Cairney, J.M. (2016) Deformation-induced trace element redistribution in zircon revealed using atom probe tomography. Nature Communications, 7, doi: 10.1038/ncomms10490.

Reddy, S.M., van Riessen, A., Saxey, D.W., Johnson, T.E., Rickard, W.D., Fougerouse, D., Fischer, S., Prosa, T.J., Rice, K.P., and Reinhard, D.A. (2016) Mechanisms of deformation-induced trace element migration in zircon resolved by atom probe and correlative microscopy. Geochimica et Cosmochimica Acta, 195, 158–170.

Ridolfi, F., Renzulli, A., and Puerini, M. (2010) Stability and chemical equilibrium of amphibole in calc-alkaline magmas: An overview, new thermobarometric formulations and application to subduction-related volcanoes. Contributions to Mineralogy and Petrology, 160, 45–66.

Salisbury, M.J., Bohrson, W.A., Clynne, M.A., Ramos, F.C., and Hoskin, P. (2008) Multiple plagioclase crystal populations identified by crystal size distribution and in situ chemical data: Implications for timescales of magma chamber processes associated with the 1915 eruption of Lassen Peak, CA. Journal of Petrology, 49, 1755–1780.

Saxey, D.W., Moser, D.E., Piazolo, S., Reddy, S.M., and Valley, J.W. (2018) Atomic worlds: Current state and future of atom probe tomography in geoscience. Scripta Materialia, 148, 115–121.

Schmidt, M.W. (1992) Amphibole composition in tonalite as a function of pressure: an experimental calibration of the Al-in-hornblende barometer. Contributions to Mineralogy and Petrology, 110, 304–310.

Sibley, D.F., Vogel, T.A., Walker, B.M., and Byerly, G.R. (1976) The origin of oscillatory zoning in plagioclase; a diffusion and growth controlled model. American Journal of Science, 276, 275–284.

Sillitoe, R.H. (2010), Porphyry copper systems. Economic Geology, 105, 3–41.

Singer, B. S., Costa, F., Herrin, J. S., Hildreth, W., and Fierstein, J. (2016) The timing of compositionally-zoned magma reservoirs and mafic ‘priming’ weeks before the 1912 Novarupta-Katmai rhyolite eruption. Earth and Planetary Science Letters, 451, 125–137.

Smith, J.V., and Ribbe, P.H. (1969) Atomic movements in plagioclase feldspars: Kinetic interpretation. Contributions to Mineralogy and Petrology, 21, 157–202.

Smith, J.V., and Brown, W.L. (1974) Feldspar minerals, 14 p. Springer-Verlag, New York.

Stamatelopoulou-Seymour, K., Vlassopoulos, D., Pearce, T.H., and Rice, C. (1990) The record of magma chamber processes in plagioclase phenocrysts at Thera Volcano, Aegean Volcanic Arc, Greece. Contributions to Mineralogy and

Petrology, 104, 73–84.

Thompson, K., Lawrence, D., Larson, D., Olson, J., Kelly, T., and Gorman, B. (2007) In situ site-specific specimen preparation for atom probe tomography. Ultramicroscopy, 107, 131–139.

Ustunisik, G., Kilinc, A., and Nielsen, R.L. (2014) New insights into the processes controlling compositional zoning in plagioclase. Lithos, 200–201, 80–93.

Valley, J.W., Cavosie, A.J., Ushikubo, T., Reinhard, D.A., Lawrence, D.F., Larson, D.J., Clifton, P.H., Kelly, T.F., Wilde, S.A., and Moser, D.E. (2014) Hadean age for a post-magma-ocean zircon confirmed by atom-probe tomography. Nature Geoscience, 7, 219–223.

Walker, D., Longhi, J., Lasaga, A.C., Stolper, E.M., Grove, T.L., and Hays, J.F. (1977) Slowly cooled microgabbros 15555 and 15065. Proceedings of the Eighth Lunar Science Conference, 1521–1547.

Waters, P.J., Cooke, D.R., Gonzales, R.I., and Phillips, D. (2011) Porphyry and epithermal deposits and ^{40}Ar/^{39}Ar geochronology of the Baguio district, Philippines. Economic Geology, 106, 1335–1363.

Wenk, H.R., and Nakajima, Y. (1980) Structure, formation, and decomposition of APB's in Calcic plagioclase. Physics and Chemistry of Minerals, 6, 169–186.

White, L.F., Darling, J.R., Moser, D.E., Reinhard, D.A., Prosa, T.J., Bullen, D., Olson, D., Larson, D.J., Lawrence, D., and Martin, I. (2017) Atomic-scale age resolution of planetary events. Nature Communications, 8, doi: 10.1038/ncomms15597.

Wilke, M., and Behrens, H. (1999) The dependence of the partitioning of iron and europium between plagioclase and hydrous tonalitic melt on oxygen fugacity. Contributions to Mineralogy and Petrology, 137, 102–114.

FIGURE CAPTIONS

FIGURE 1. (**a**) Scan of whole thin section and (**b**) sketch of the phenocryst

assemblage of plagioclase and amphibole showing the position of the analyzed plagioclase. Plagioclase crystals are colored in pink and amphibole crystals in green in **b**, the scale bar is 0.5 cm in **a** and **b**. (**c**) Representative photomicrograph showing amphibole inclusions in the plagioclase phenocryst with enlargement of amphibole (plane-polarized light). (**d**) Backscattered electron (BSE) image showing the amphibole inclusions and complex texture of the patchy core, Ca-rich mantle and oscillatory zoned rim, the location of EMP, LA-ICPMS and APT specimens 1 and 2 analytical targets in plagioclase. Scanning electron microscope images of needle-shaped specimens APT 1 and 2 with representative EMP (An) values illustrated in **d**. Abbreviations: Am, amphibole; Pl, plagioclase.

FIGURE 2. (**a**) Backscattered electron (BSE) image and (**b**, **c**) X-ray maps of Ca and Na showing the texture and EMP analysis position in plagioclase. (**d**, **e**, **f**, **g**, **h**) Profile variations of SiO_2, CaO, Al_2O_3, Na_2O and K_2O contents (wt%) analyzed by EMP. (**i**) Profile An (mol%) variations. The insert figures in **d** to **i** are the BSE images of EMP analysis position.

FIGURE 3. Profile of elemental variations (in ppm) from core to rim as determined by LA-ICPMS. The gray area shows the Ca-rich mantle zone. The insert figures are bottom are the BSE images of LA-ICPMS analysis position.

FIGURE 4. Atom probe mass spectrum. Peaks are colour-coded by atomic or molecular species.

FIGURE 5. Reconstruction of atom probe data for specimen 1 showing Na (**a**), Ca (**b**) and (Na+Si)/(Al+Ca) atomic ratio isosurface (**c**) with the position of cylinder profile.

(**d**, **e**, **f**, **g**, **h**) Cylinder profile Al, Ca, Na and Si (atomic concentration %) and the ratios of Ca/(Ca+Na) showing the nano-scale variations of Al, Ca, Na, Si and Ca/(Ca+Na).

FIGURE 6. Reconstruction of atom probe data for sample 2 showing homogenous Na (green dot) and Ca (red dot) distribution.

FIGURE 7. (**a**) Crystallization temperature (ºC) of amphibole inclusions in plagioclase and independent phenocrysts estimated by amphibole thermometry (Ridolfi et al., 2010) compared with previously published thermometry on zircon and co-existing magnetite-ilmenite in the groundmass (Cao et al. 2018a), indicating the early mineral phases were amphibole, followed by groundmass amphibole and the late mineral phases of zircon and co-existing magnetite-ilmenite. (**b**) Plot of crystallization temperature (ºC) versus pressure (kbar) for amphibole estimated by amphibole thermometry (Ridolfi et al. 2010) and the Al-in-hornblende geobarometer (Schmidt 1992) showing two slightly different groups. (**c**) Plot of temperature (ºC) versus log$f$O$_2$ for amphibole with previously published data for co-existing magnetite-ilmenite (Cao et al. 2018a) indicating relatively oxidized conditions and limited variations of oxygen fugacity from the early to late stage of magma formation. Abbreviations: Am, amphibole; Ilm, ilmenite; Mag, magnetite; Pl, plagioclase; Zrc, zircon; HM, Fe_2O_3–Fe_3O_4 buffer; NNO, Ni–NiO buffer, QFM, SiO_2–Fe_2SiO_4–Fe_3O_4 buffer.

FIGURE 8. Zircon $^{206}Pb/^{238}U$ age (Ma) with 2σ uncertainty for syn-mineralization diorite porphyry analyzed by chemical abrasion-isotope dilution-thermal ionization

mass spectrometry (ID-TIMS) from Hollings et al. (2013). The inset shows the zircon crystallization temperatures with 2σ uncertainty of ~15 ºC according to Ti-in-zircon thermometry of Ferry and Watson (2007) on the data of Cao et al. (2018a).

FIGURE 9. Two distinct cooling rates (ºC/year) calculated from to micro- and nano-scale zoning in plagioclase with minimum cooling rate of 0.0005 for magmatic stage with T > 680 ºC and a higher minimum cooling rate of 0.26 after emplacement. Inset figures are BSE images of analyzed plagioclase, enlarged BSE image showing the micro-scale oscillatory zoning and reconstruction from Figure 5 showing the nano-scale zoning. See text for details.

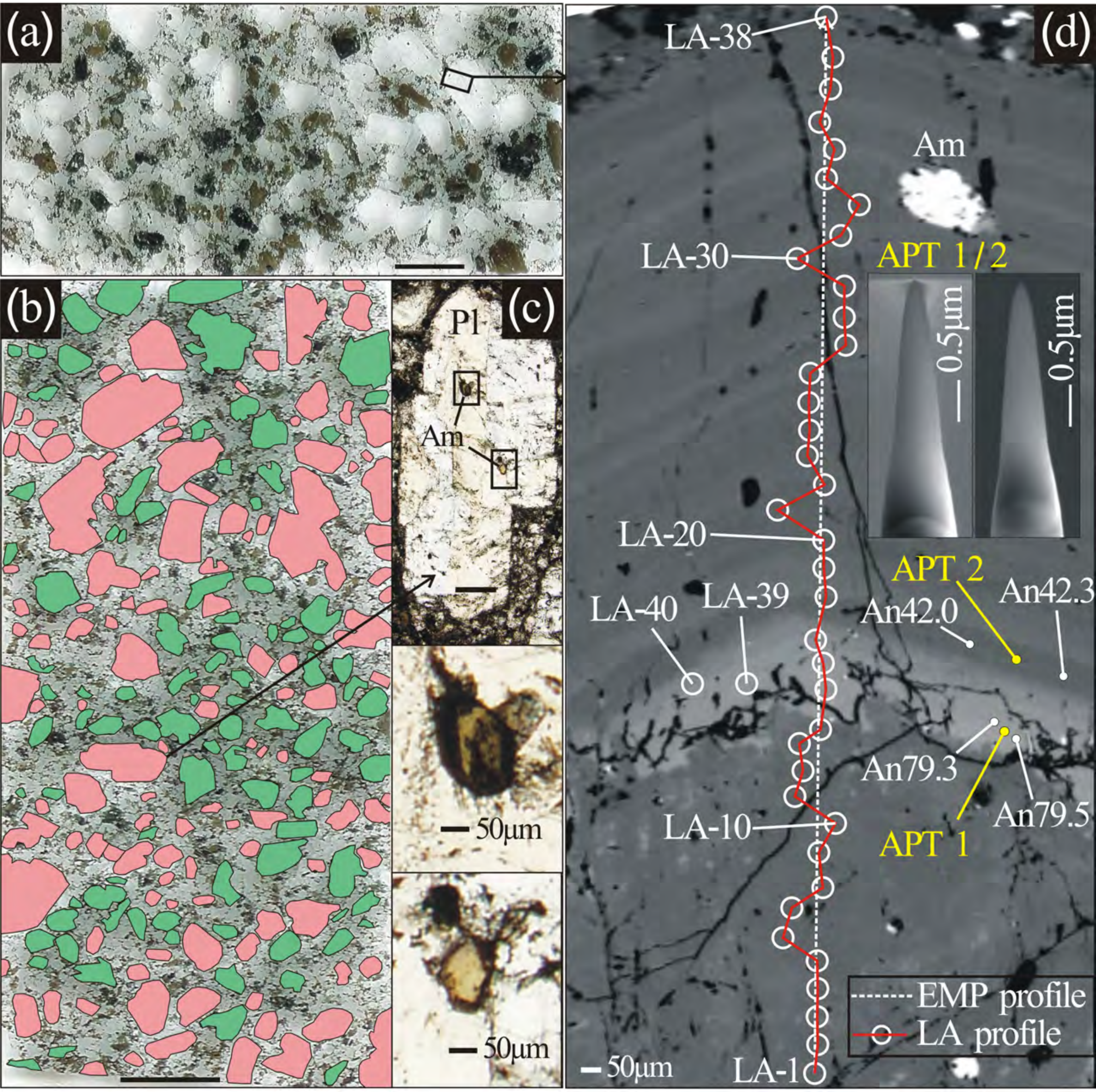
(a)
(b)
(c)
Pl
Am
50μm
50μm
(d)
LA-38
Am
LA-30
APT 1 / 2
0.5μm
0.5μm
LA-20
APT 2
LA-40
LA-39
An42.0
An42.3
An79.3
An79.5
LA-10
APT 1
EMP profile
LA profile
50μm
LA-1

Fig. 1

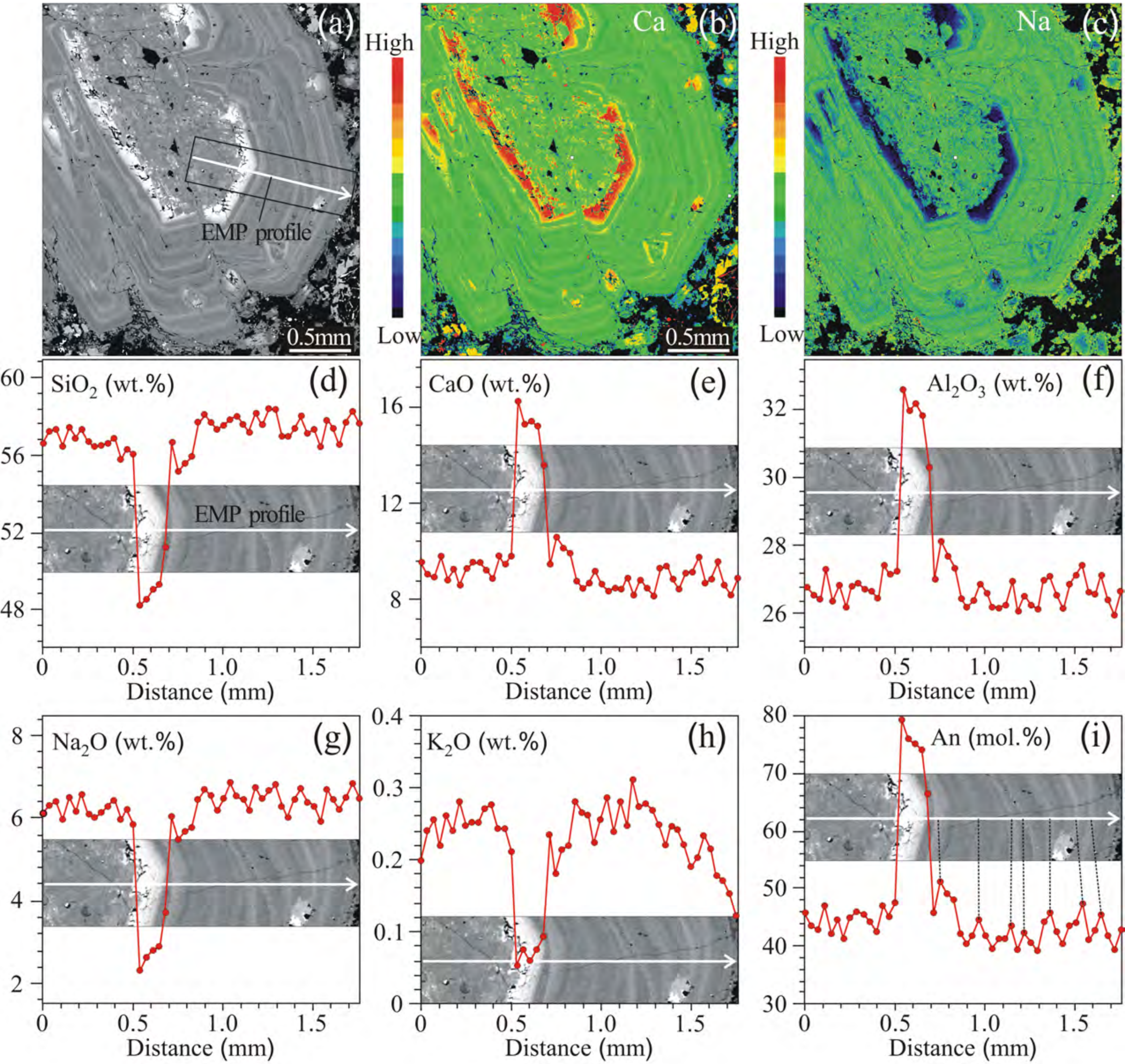

(a)
EMP profile
0.5mm
Ca
(b)
High
Low
0.5mm
Na
(c)
High
Low
SiO2 (wt.%)
(d)
60
56
52
48
EMP profile
CaO (wt.%)
(e)
16
12
8
Al2O3 (wt.%)
(f)
32
30
28
26
Na2O (wt.%)
(g)
8
6
4
2
K2O (wt.%)
(h)
0.4
0.3
0.2
0.1
0
An (mol.%)
(i)
80
70
60
50
40
30
0
0.5
1.0
1.5
Distance (mm)

Fig. 2

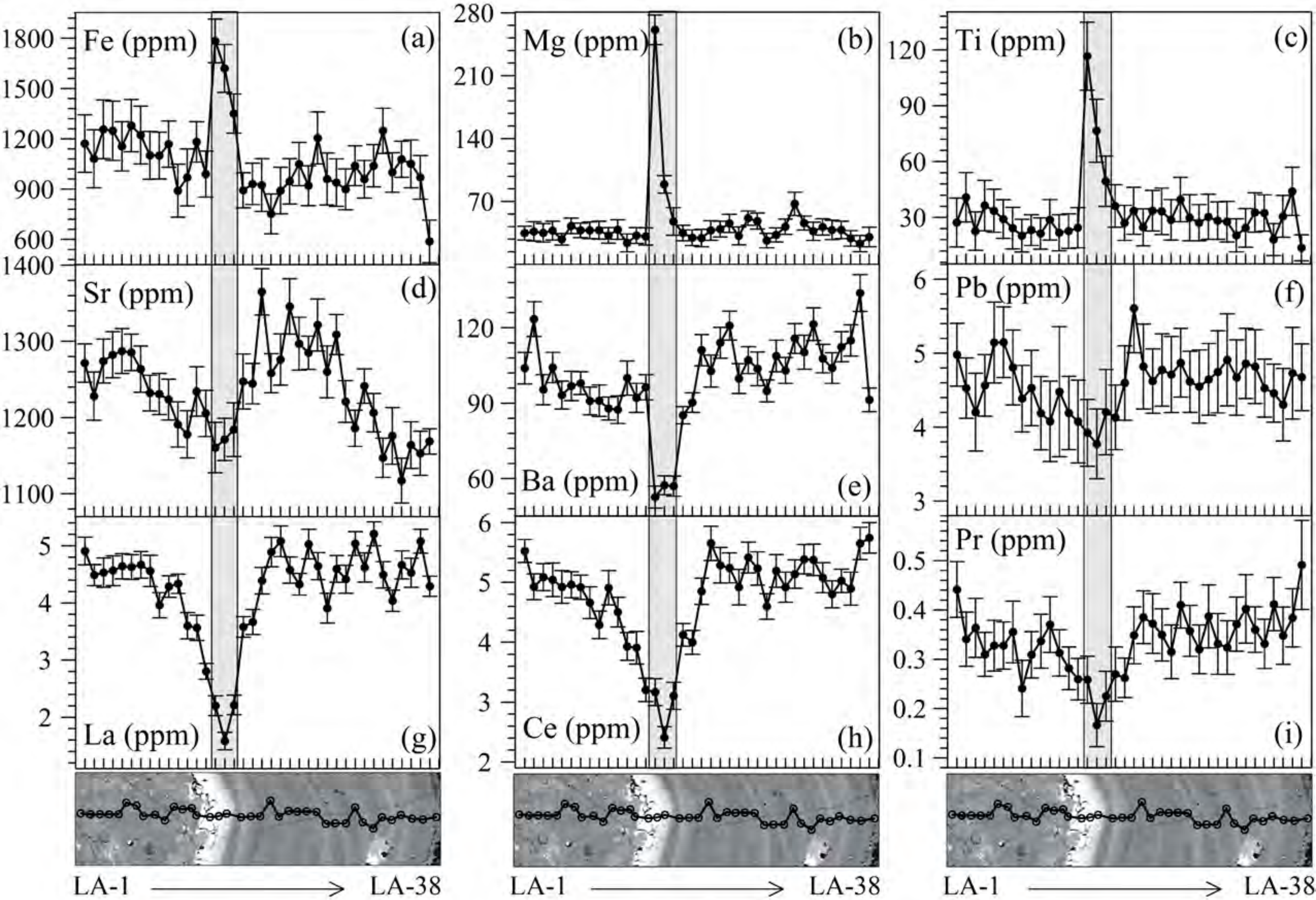

Fe (ppm)
(a)
1800
1500
1200
900
600
Mg (ppm)
(b)
280
210
140
70
Ti (ppm)
(c)
120
90
60
30
Sr (ppm)
(d)
1400
1300
1200
1100
Ba (ppm)
(e)
120
90
60
Pb (ppm)
(f)
6
5
4
3
La (ppm)
(g)
5
4
3
2
Ce (ppm)
(h)
6
5
4
3
2
Pr (ppm)
(i)
0.5
0.4
0.3
0.2
0.1
LA-1
LA-38

Fig. 3

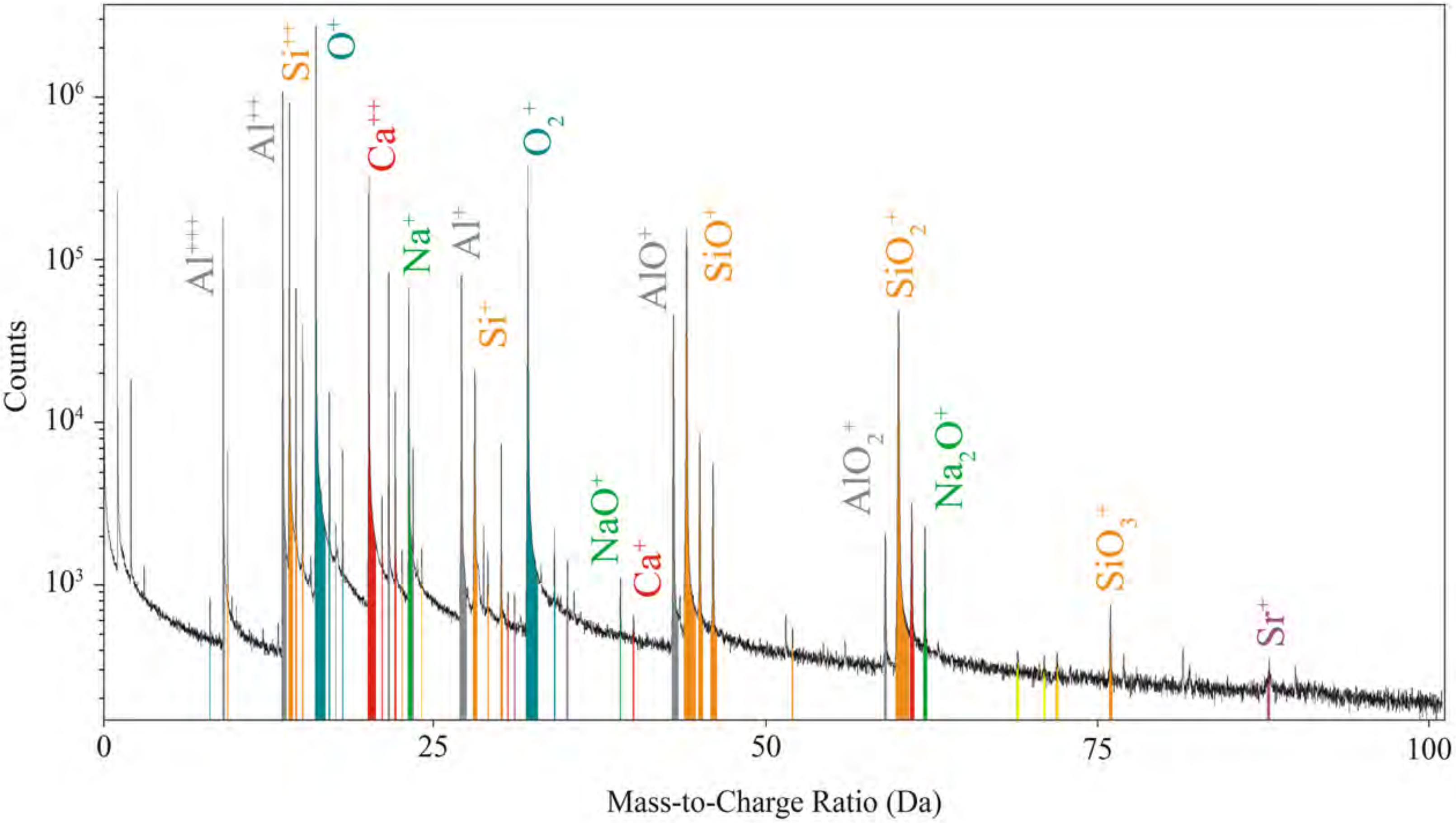
Al+++
Al++
Si++
O+
Ca++
O2+
Na+
Al+
Si+
AlO+
SiO+
SiO2+
AlO2+
Na2O+
NaO+
Ca+
SiO3+
Sr+
Counts
10^6
10^5
10^4
10^3
0
25
50
75
100
Mass-to-Charge Ratio (Da)

Fig. 4

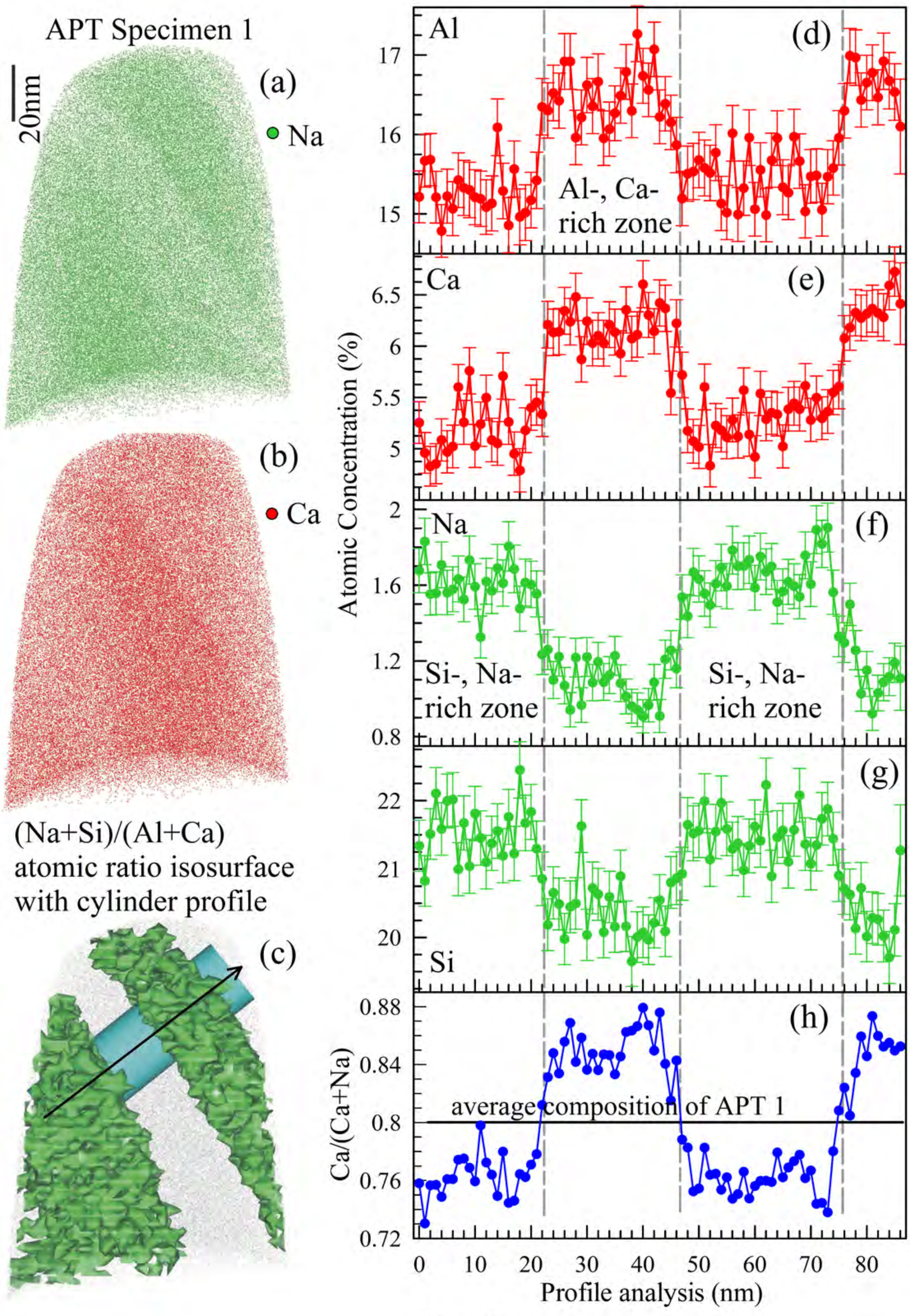
APT Specimen 1
20nm
(a)
Na
(b)
Ca
(Na+Si)/(Al+Ca)
atomic ratio isosurface
with cylinder profile
(c)
Al
(d)
17
16
15
Al-, Ca-
rich zone
Ca
(e)
6.5
6
5.5
5
Atomic Concentration (%)
Na
(f)
2
1.6
1.2
0.8
Si-, Na-
rich zone
Si-, Na-
rich zone
(g)
22
21
20
Si
(h)
0.88
0.84
0.8
0.76
0.72
Ca/(Ca+Na)
average composition of APT 1
0
10
20
30
40
50
60
70
80
Profile analysis (nm)

Fig. 5

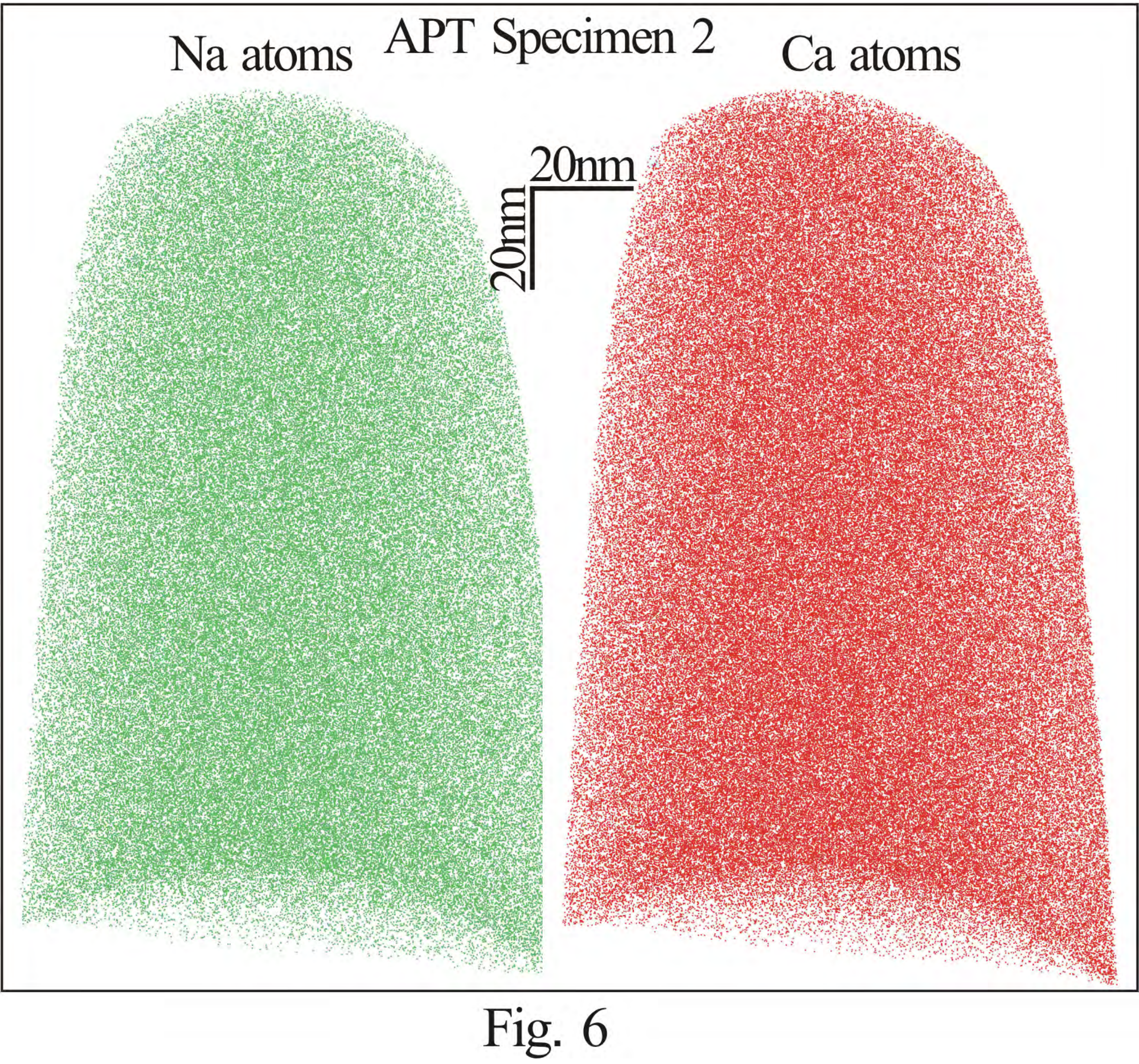

Fig. 6

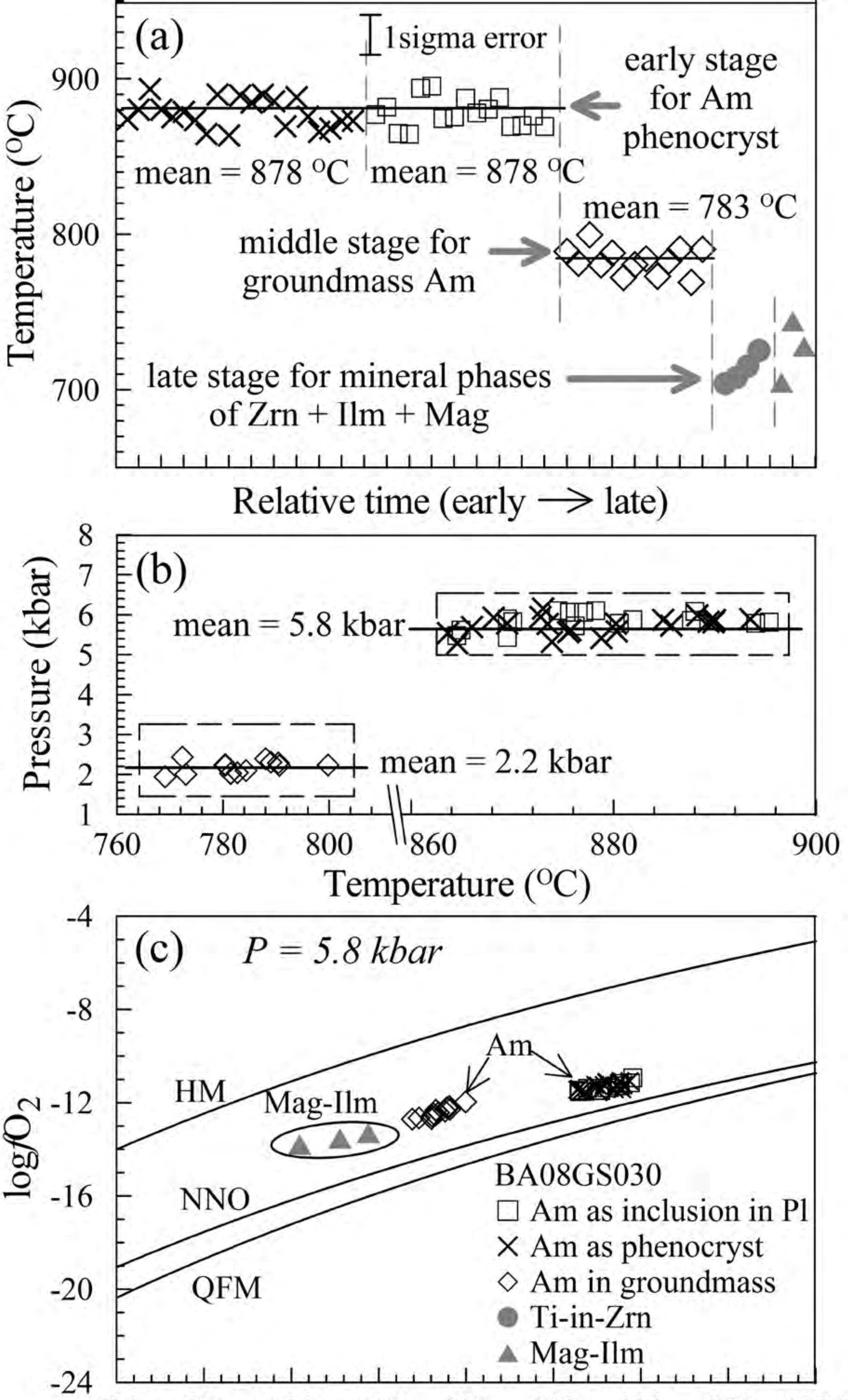
(a)
1sigma error
early stage for Am phenocryst
mean = 878 °C
mean = 878 °C
mean = 783 °C
middle stage for groundmass Am
late stage for mineral phases of Zrn + Ilm + Mag
Temperature (°C)
900
800
700
Relative time (early → late)
(b)
mean = 5.8 kbar
mean = 2.2 kbar
Pressure (kbar)
8
7
6
5
4
3
2
1
760
780
800
860
880
900
Temperature (°C)
(c)
P = 5.8 kbar
HM
NNO
QFM
Mag-Ilm
Am
BA08GS030
□ Am as inclusion in Pl
× Am as phenocryst
◇ Am in groundmass
● Ti-in-Zrn
▲ Mag-Ilm
log fO2
-4
-8
-12
-16
-20
-24
600
650
700
750
800
850
900
950
1000
Temperature (°C)

Fig. 7

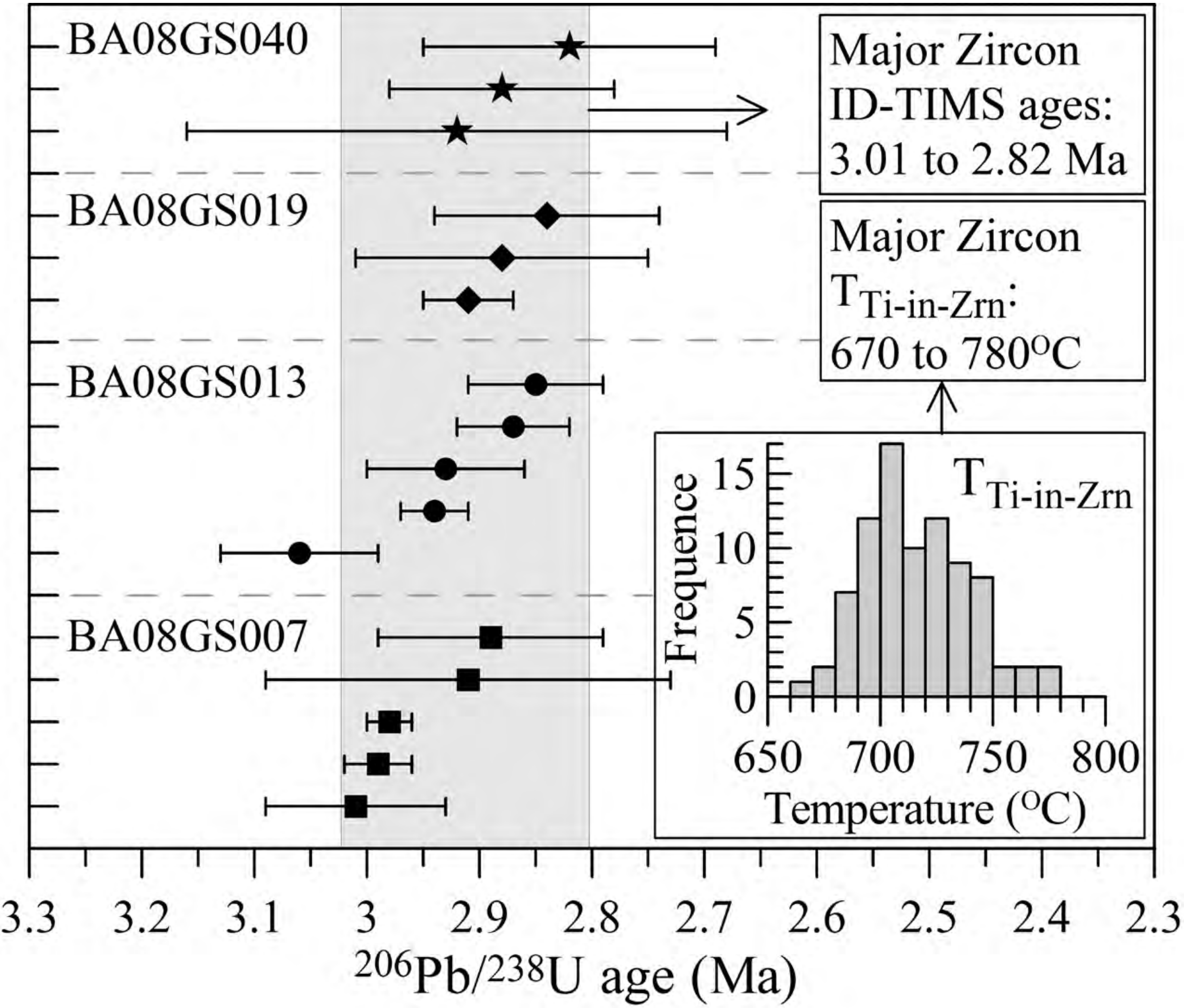
BA08GS040
BA08GS019
BA08GS013
BA08GS007
Major Zircon ID-TIMS ages: 3.01 to 2.82 Ma
Major Zircon $T_{Ti-in-Zrn}$: 670 to 780^{O}C
$T_{Ti-in-Zrn}$
Frequence
0
5
10
15
650
700
750
800
Temperature (^{O}C)
3.3
3.2
3.1
3
2.9
2.8
2.7
2.6
2.5
2.4
2.3
^{206}Pb/^{238}U age (Ma)

Fig. 8

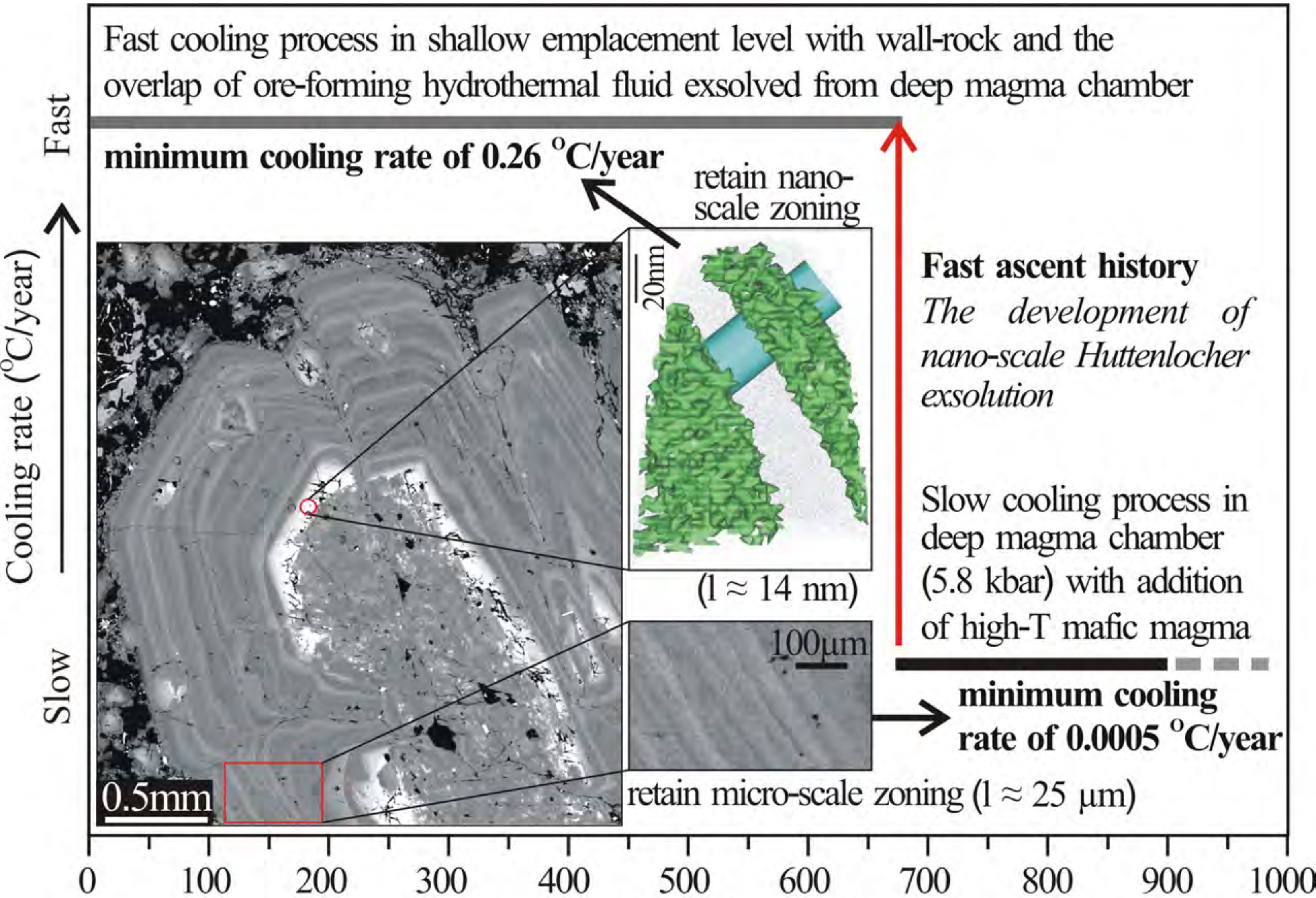
Fast cooling process in shallow emplacement level with wall-rock and the overlap of ore-forming hydrothermal fluid exsolved from deep magma chamber
minimum cooling rate of 0.26 ^{o}C/year
retain nano-scale zoning
20nm
(l ≈ 14 nm)
Fast ascent history
The development of nano-scale Huttenlocher exsolution
Slow cooling process in deep magma chamber (5.8 kbar) with addition of high-T mafic magma
100μm
minimum cooling rate of 0.0005 ^{o}C/year
retain micro-scale zoning (l ≈ 25 μm)
0.5mm
Fast
Slow
Cooling rate (^{o}C/year)
0
100
200
300
400
500
600
700
800
900
1000
Crystallization T(^{o}C)

Fig. 9